Tubuloglomerular Feedback-Mediated Dynamics in Three Coupled Nephrons[1]

Tracy L. Stepien[2]

Advisor: E. Bruce Pitman[3]

Abstract

A model of three coupled nephrons branching from a common cortical radial artery is developed to further understand the effects of equal and unequal coupling on tubuloglomerular feedback. The integral model of Pitman *et al.* (2002), which describes the fluid flow up the thick ascending limb of a single, short-looped nephron of the mammalian kidney, is extended to a system of three nephrons through a model of coupling proposed by Pitman *et al.* (2004). Analysis of the system, verified by numerical results, indicates that stable limit-cycle oscillations emerge for sufficiently large feedback gain magnitude and time delay through a Hopf bifurcation, similar to the single nephron model, yet generally at lower values. Previous work has demonstrated that coupling induces oscillations at lower values of gain, relative to uncoupled nephrons. The current analysis extends this earlier finding by showing that asymmetric coupling among nephrons further increases the likelihood of the model nephron system being in an oscillatory state.

1 Introduction

1.1 Kidneys and Nephrons

The human kidneys are two bean-shaped organs with one on each side of the vertebral column. Functions of the kidneys include regulating water and electrolyte balance, excretion of metabolic waste products and foreign chemicals, gluconeogenesis, and secretion of hormones. There are two main regions in the kidney: the renal cortex, the outer region of the kidney, and the renal medulla, the inner region (refer to Appendix A or Vander (1995) for further detail).

The principal functioning unit of the mammalian kidney is the nephron, an S-shaped tubule which filters blood by reabsorbing necessary nutrients and excreting waste as urine. Each human kidney contains approximately one million nephrons and rat kidneys contain approximately forty-thousand nephrons each. The filtering component of every nephron is located in the renal cortex and the tubule component of each nephron extends to either the outer or inner renal medulla, depending on their length. Short-looped nephrons extend only to the outer renal medulla, while long-looped nephrons extend further to the inner renal medulla.

Blood enters a nephron through the afferent arteriole, which branches off a cortical radial artery (refer to Figure 1 for the approximate anatomy of a nephron). It then flows to the glomerulus, a tuft of capillaries surrounded by Bowman's capsule, and then returns to general circulation through the efferent arteriole. Glomerular filtration begins as fluid flows from the glomerulus into Bowman's

[1]Presented in preliminary form at the University at Buffalo Applied Mathematics Seminar and the University at Buffalo Celebration of Academic Excellence, Buffalo, NY, and Undergraduate Biomathematics Day, Niagara Falls, NY.

[2]Department of Mathematics, State University of New York, Buffalo, NY 14260-2900, U.S.A.
Present address: Department of Mathematics, University of Pittsburgh, Pittsburgh, PA 15260, U.S.A. (tls52@pitt.edu)

[3]Department of Mathematics, State University of New York, Buffalo, NY 14260-2900, U.S.A. (pitman@buffalo.edu)

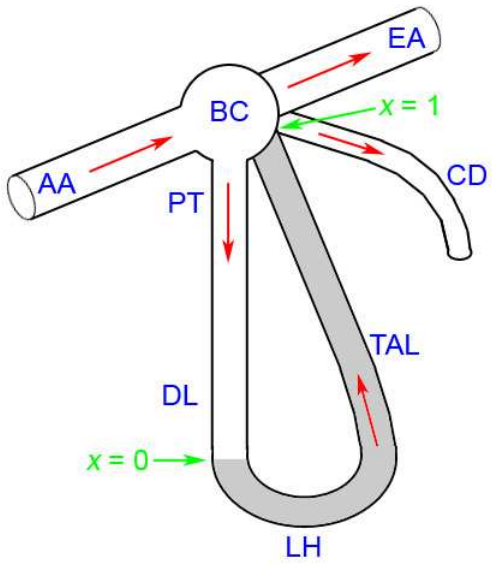

Figure 1: Schematic drawing of a short-looped nephron: Afferent arteriole (AA), efferent arteriole (EA), Bowman's capsule (BC), proximal tubule (PT), descending limb (DL), Loop of Henle (LH), thick ascending limb (TAL), and collecting duct (CD). The glomerulus is located within Bowman's capsule, and the distal tubule is the tubular segment between the TAL and the collecting duct. The macula densa is actually on the back side of the TAL and adjacent to the region where the glomerulus, afferent arteriole, and efferent arteriole come together. Red arrows represent the flow direction.

capsule. Glomerular membranes are permeable to water and crystalloids and relatively permeable to colloids, so the flow consists of essentially protein-free plasma. This filtrate flows down through the proximal tubule into the descending limb of the Loop of Henle where the composition alters while water is passively reabsorbed into the interstitium. Then the filtrate continues to flow up the thick ascending limb (TAL) where the composition alters again while sodium and chloride are reabsorbed by means of active transport and diffusion.

Fluctuations in blood pressure can result from many physiological sources including heart beating, breathing, stress, activity, or other events, causing perturbations in renal blood flow. The glomerular filtration rate is then affected by this change in flow because an increase in blood pressure causes an increase in blood flow rate, which causes an increase in glomerular filtration rate, and therefore causes an increase in the concentration of sodium and chloride in the fluid. A form of renal regulation is responsible for counteracting the effects of blood pressure changes.

As fluid flows from the TAL to the distal tubule, it flows through the macula densa, a plaque of specialized cells in the wall of the TAL, where the concentration of sodium and chloride in the fluid is sensed. The macula densa is stimulated by an increase or decrease in sodium and chloride concentration, and a chemical signal is directed toward the afferent arteriole causing the arteriole to constrict or dilate, respectively. This adjustment is tubuloglomerular feedback (TGF), which results in a change in the blood flow and hydrostatic pressure within the glomerulus, and therefore a change in glomerular filtration rate in the nephron. TGF serves a role in renal autoregulation by stabilizing renal blood flow and glomerular filtration rate to prevent large changes in blood flow, which could result from systemic arterial blood pressure fluctuations.

1.2 Previous Experimental Findings

Oscillations in single nephron glomerular filtration rate, TAL fluid chloride concentration, tubular fluid flow rate, and intratubular fluid pressure have been observed in experiments in normotensive rats as well as dogs (Leysaac and Baumbach, 1983; Leysaac, 1986; Holstein-Rathlou and Marsh, 1989; Holstein-Rathlou and Marsh, 1994; Just *et al.*, 1998). These oscillations have been determined to be related to TGF; limit-cycle oscillations are approximated in most cases and have a frequency of 20-50 mHz. Irregular, and perhaps chaotic, oscillations have also been observed in experiments in hypertensive rats (Holstein-Rathlou and Leysaac, 1986; Yip *et al.*, 1991). The lack of knowledge

regarding the exact causes and effects of these oscillations has led to further investigations.

Numerous mathematical models based on rat nephrons have been developed to clarify the emergence of flow oscillations (Holstein-Rathlou and Leysaac, 1987; Pitman and Layton, 1989; Holstein-Rathlou and Marsh, 1990; Layton *et al.*, 1991; Barfred *et al.*, 1996; Pitman *et al.*, 2002; Pitman *et al.*, 2004; Layton *et al.*, 2006). Single nephron models predict a Hopf bifurcation from a stable, time-independent steady state to limit-cycle oscillations and an unstable state when parameters cross a bifurcation locus in the feedback-loop gain–time delay parameter plane (Layton *et al.*, 1991).

Anatomical and physiological observations indicate that nephrons can be significantly influenced by events in neighboring nephrons. Studies by Casellas *et al.* (1994) indicate that most nephrons are organized in pairs and triplets branching from a common cortical radial artery, and this vascular tree organization is found in many mammals. Holstein-Rathlou (1987), Källskog and Marsh (1990), Yip *et al.* (1992), and Chen *et al.* (1995) observed that perturbations in fluid flow in one nephron can propagate to a paired nephron, and the resulting flow oscillations are usually synchronous and nearly in-phase. Coupling of relatively close nephrons via vascular pathways is strongly supported by these experimental studies.

In Pitman *et al.* (2004), a model of coupling between two nephrons and its effect on TGF-mediated dynamics was analyzed. It was demonstrated that symmetric coupling induces oscillations at lower values of gain, relative to uncoupled nephrons. However, since nephrons have been observed coupled in triplets as well, a question arises: how are TGF-mediated dynamics affected by asymmetric coupling between three nephrons?

A model of three coupled nephrons branching from a common cortical radial artery is developed and analyzed in this study to further understand the effects of coupling on nephron fluid flow oscillations in TGF. The model is based on the single nephron integral model of Pitman *et al.* (2002) and the model of coupling proposed by Pitman *et al.* (2004).

2 Previous Modeling of Nephrons

In this section, the following previous models will be summarized: the 1-nephron integral model of Pitman *et al.* (2002) derived from the PDE model of Layton *et al.* (1991), the 2-nephron model of Pitman *et al.* (2004), and the N-nephron model of Bayram (2006).

2.1 1-Nephon Model

The single nephron integral model is representative of a short-loop nephron found in rats. A nephron of this size would extend from the boundary of the outer medulla to the boundary of the cortex. The model assumes that the TAL is an impermeable rigid tube, the descending limb of the Loop of Henle is infinitely permeable to water, the addition of sodium chloride (NaCl) to the interstitium does not alter the concentration in that location, and solute backleak is zero (see Pitman *et al.*, 2002).

The equation for the integral model is expressed in nondimensional form. In this representation of TGF, the space variable x is set such that $x = 0$ is the location of the entrance of the TAL, and $x = 1$ is the macula densa. Referencing Figure 1, the section of the nephron that is being modeled is located in the outer medulla and the cortex, and it extends from the bend of the Loop of Henle to the macula densa.

Define $T_x(t)$ as the TAL transit time from $x = 0$ to a position $x \in [0, 1]$ at time t. Therefore, it takes a particle entering the TAL at $x = 0$ and moving with the flow in the modeled TAL a time $T_x(t)$ to reach a location x at time t. Using the relation between distance and speed, the location

of a particle is found by integrating the TAL intratubular fluid speed $\mathcal{F}$ over the time spent flowing from 0 to x, which results in an implicit equation for $T_x(t)$,

$$x(t) = \int_{t-T_x(t)}^{t} \mathcal{F}(s)ds, \tag{1}$$

where $t - T_x(t)$ is the time at which the particle currently located at x entered the TAL at $x = 0$. By evaluating Equation 1 at $x = 1$ and defining the transit time from $x = 0$ (the entrance of the TAL) to $x = 1$ (the macula densa) as $T_{MD}(t) \equiv T_1(t)$, one obtains

$$1 = \int_{t-T_{MD}(t)}^{t} \mathcal{F}(s)ds. \tag{2}$$

This is defined as the steady state solution where the transit time between the entrance of the TAL and the macula densa is 1. It is assumed that the flow speed $\mathcal{F}$ can differ from the steady state by no more than a small amount ϵ, where $0 \leq \epsilon < 1$. This means that the flow speed $\mathcal{F}$ is always positive with $(1 - \epsilon) \leq \mathcal{F} \leq (1 + \epsilon)$.

To solve for $T_{MD}(t)$, a linearization is required. Let $x = g(T_x(t))$ in Equation 1, such that

$$g(T_x(t)) = \int_{t-T_x(t)}^{t} \mathcal{F}(s)ds. \tag{3}$$

Setting $x = 1$ so that $T_x(t) = T_{MD}(t)$,

$$1 = g(T_{MD}(t)) = \int_{t-T_{MD}(t)}^{t} \mathcal{F}(s)ds, \tag{4}$$

and then expanding $g(T_{MD}(t))$ in a Taylor series to first order about $T_{MD}(t) = 1$ (with t considered fixed) results in

$$\begin{aligned} 1 = g(T_{MD}(t)) &\approx g(1) + (T_{MD}(t) - 1)g'(1) \\ 1 &\approx \int_{t-1}^{t} \mathcal{F}(s)ds + (T_{MD}(t) - 1)\mathcal{F}(t-1). \end{aligned} \tag{5}$$

Solving Equation 5 for $T_{MD}(t)$ results in

$$T_{MD}(t) \approx 1 + \frac{1 - \int_{t-1}^{t} (\mathcal{F}(s))ds}{\mathcal{F}(t-1)} = 1 + \frac{\int_{t-1}^{t} (1 - \mathcal{F}(s))ds}{\mathcal{F}(t-1)}. \tag{6}$$

To determine the form of the flow rate $\mathcal{F}$, we use an equation obtained empirically by physiologists that represents the feedback response (see Layton *et al.*, 1991) which, as a result of linearization, is

$$\mathcal{F}(t) \approx 1 + K_1 \tanh\left(K_2 \left(T_{MD}(t - \tau) - 1\right)\right). \tag{7}$$

In this equation, τ is the positive delay time between a change in concentration at the macula densa and the full response of the afferent arteriole constriction or dilation. The positive constants K_1 and K_2 describe, respectively, the range of the feedback response and its sensitivity to deviations from the steady state. K_1 is equal to $\frac{\Delta Q}{2C_{op}}$, where ΔQ is the difference between maximum and minimum single nephron glomerular filtration rate (see Figure 2), and (C_{op}, Q_{op}) is the steady state operating point. K_2 is equal to $\frac{kC_0}{2}$, where k is a scaling coefficient for TGF response and C_0 is

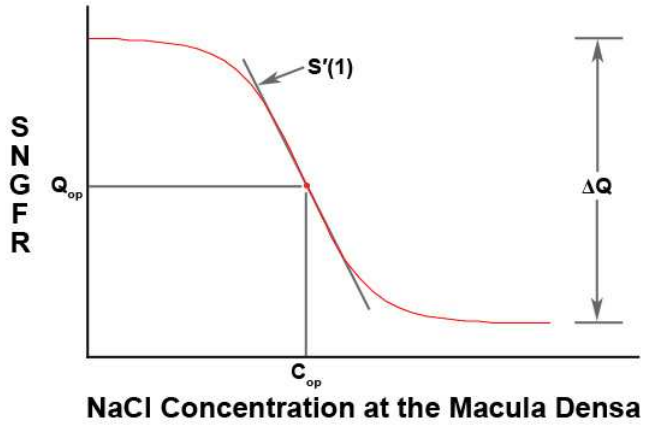

Figure 2: Sigmoidal relationship between single nephron glomerular filtration rate (SNGFR) and sodium chloride (NaCl) concentration at the macula densa: (C_{op}, Q_{op}) is the steady state operating point, ΔQ is the difference between maximum and minimum single nephron glomerular filtration rate, and $S'(1)$ is the magnitude of the slope of the tangent line to the curve at the steady state operating point.

the chloride concentration at the loop bend.

We define the parameter γ as the gain magnitude of the feedback loop, which is a measure of the signal amplification by the feedback loop. γ is related to K_1 and K_2 by the equation

$$\gamma = K_1 K_2[-S'(1)]. \tag{8}$$

Multiplied together, K_1K_2 is a measure of the strength of the feedback response at the renal corpuscle and macula densa. $-S'(1)$ is the magnitude of the slope of the steady-state chloride concentration profile at the macula densa (see Figure 2). As a result of the linearization used to obtain Equation 7, the value of $-S'(1)$ cancels, and substituting $K_2 = \frac{\gamma}{K_1}$ into Equation 7 results in

$$\mathcal{F}(t) \approx 1 + K_1 \tanh\left(\frac{\gamma}{K_1}\left(T_{MD}(t-\tau) - 1\right)\right). \tag{9}$$

From here, Equation 6 can be substituted into Equation 9, resulting in the single nephron integral model,

$$\mathcal{F}(t) = 1 + K_1 \tanh\left(\frac{\gamma \int_{t-\tau-1}^{t-\tau}(1-\mathcal{F}(s))ds}{K_1 \mathcal{F}(t-\tau-1)}\right). \tag{10}$$

This equation expresses the nondimensionalized TAL flow rate $\mathcal{F}$ at time t as a function of average flow over a fixed interval of time. Based on estimates of Layton *et al.* (1991), the typical nondimensional range of the time delay is assumed to be $\tau \in [0.13, 0.37]$ and the typical nondimensional range of the gain is assumed to be $\gamma \in [1.5, 3.6]$.

The integral model is a linearization of the characteristic form of the hyperbolic PDE model of Layton *et al.* (1991) that was derived by using the method of characteristics. A comparison of the two models indicates that for moderate values of γ and τ, results are very similar. For larger values of γ and τ, the integral model deviates slightly from the PDE model. However, the characteristic equation for the bifurcation curve for both models is exactly the same (Pitman *et al.*, 2002). Due to the similarities between the two models, the integral model is chosen as the basis for the three coupled nephrons model because it is more computationally manageable than the PDE model.

2.2 2-Nephron Model

While many nephrons physiologically appear as uncoupled single nephrons, studies by Casellas *et al.* (1994) indicate that approximately 50% of nephrons are organized in pairs and triplets. The nephrons' afferent arterioles branch off a common cortical radial artery, and this vascular tree

organization is found in many mammals including humans, rats, and dogs, as well as in several amphibian species.

Holstein-Rathlou (1987), Källskog and Marsh (1990), Yip *et al.* (1992), and Chen *et al.* (1995) observed that perturbations of fluid flow in one nephron can propagate to another nephron if they share a common origin. Casellas *et al.* (1994) determined that the minimum distance a signal would have to propagate to influence another nephron is approximately 300μm. For unpaired nephrons branching from different cortical radial arteries, the signal would need to travel through additional vessels such that the distance would be too great for perturbations to have an effect on other nephrons.

To model the behavior of nephrons organized in pairs, a positive coupling constant ϕ is introduced in the flow equation to represent the feedback component from another nephron (Pitman *et al.*, 2004). This constant is assumed to be symmetric, i.e. the effect of the i^{th} nephron on the j^{th} nephron is equal to the effect of the j^{th} on the i^{th}, or $\phi_{ij} = \phi_{ji}$. If two nephrons are uncoupled, the equations for each will be copies of Equation 10, where each nephron has its own time delay τ_1 and τ_2; gain γ_1 and γ_2; and range of feedback response K_{11} and K_{12}. If two nephrons are coupled, the equations have two terms each: the first representing the feedback component of that particular nephron, and the second representing the feedback component of the other nephron,

$$\begin{aligned} \mathcal{F}_1(t) &= F(\mathcal{F}_1(t)) + \phi\left[F(\mathcal{F}_2(t)) - 1\right] \\ \mathcal{F}_2(t) &= F(\mathcal{F}_2(t)) + \phi\left[F(\mathcal{F}_1(t)) - 1\right], \end{aligned} \tag{11}$$

where $F(\mathcal{F}_j(t))$ represents the form of $\mathcal{F}(t)$ in Equation 10. Based on experimental data obtained by Källskog and Marsh (1990) and Chen *et al.* (1995), the typical nondimensional range of the coupling constant, depending on the normalization used, is assumed to be $\phi \in [0.01, 0.30]$.

This system of equations was extended to an N-nephron model with equal coupling developed by Bayram (2006), where

$$\begin{aligned} \mathcal{F}_1(t) &= F(\mathcal{F}_1(t)) + \phi\left[F(\mathcal{F}_2(t)) - 1\right] \\ \mathcal{F}_j(t) &= F(\mathcal{F}_j(t)) + \phi\left[F(\mathcal{F}_{j-1}(t)) - 1\right] + \phi\left[F(\mathcal{F}_{j+1}(t)) - 1\right], j = 2, 3, \ldots, N-1 \\ \mathcal{F}_N(t) &= F(\mathcal{F}_N(t)) + \phi\left[F(\mathcal{F}_{N-1}(t)) - 1\right]. \end{aligned} \tag{12}$$

We use this as our basis for modeling three coupled nephrons. The system of equations can be easily deduced, and the formation of the model is described in the following section.

3 Formation of the 3-Nephron Model

Based on the nephron coupling model described previously, three nephrons are coupled together using the single nephron integral model of Pitman *et al.* (2002). Physiologically, these nephrons branch off afferent arterioles connected to a common cortical radial artery (see Figure 3). Following the system of equations of the N-nephron model developed by Bayram (2006) in Equation 12, we write the system of equations for three coupled nephrons as

$$\begin{aligned} \mathcal{F}_1(t) &= F(\mathcal{F}_1(t)) + \phi\left[F(\mathcal{F}_2(t)) - 1\right] \\ \mathcal{F}_2(t) &= F(\mathcal{F}_2(t)) + \phi\left[F(\mathcal{F}_1(t)) - 1\right] + \phi\left[F(\mathcal{F}_3(t)) - 1\right] \\ \mathcal{F}_3(t) &= F(\mathcal{F}_3(t)) + \phi\left[F(\mathcal{F}_2(t)) - 1\right]. \end{aligned} \tag{13}$$

However, we are interested in the effects of asymmetric coupling, so we define ϕ_{12} as the coupling

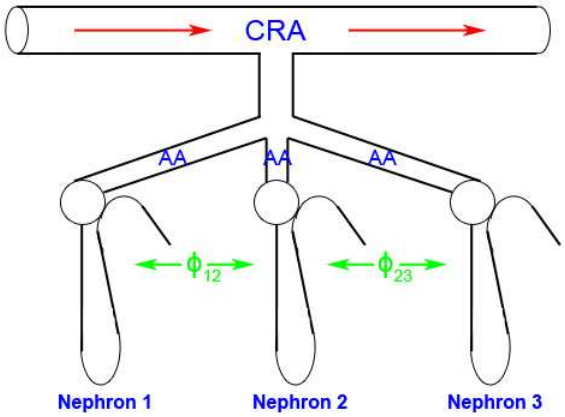

Figure 3: Schematic drawing of 3 short-looped nephrons: Each nephron's afferent arteriole (AA) branches from a common cortical radial artery (CRA). Red arrows represent the flow direction and green arrows indicate the coupling constant between nephron 1 and 2, and the coupling constant between nephron 2 and 3.

constant between the first and second nephron and ϕ_{23} as the coupling constant between the second and third nephron where $\phi_{12} \neq \phi_{23}$. We do assume that the coupling constants themselves are symmetric, i.e. $\phi_{12} = \phi_{21}$ and $\phi_{23} = \phi_{32}$. The system of equations then becomes

$$\begin{aligned}
\mathcal{F}_1(t) &= F(\mathcal{F}_1(t)) + \phi_{12}\left[F(\mathcal{F}_2(t)) - 1\right] \\
\mathcal{F}_2(t) &= F(\mathcal{F}_2(t)) + \phi_{12}\left[F(\mathcal{F}_1(t)) - 1\right] + \phi_{23}\left[F(\mathcal{F}_3(t)) - 1\right] \\
\mathcal{F}_3(t) &= F(\mathcal{F}_3(t)) + \phi_{23}\left[F(\mathcal{F}_2(t)) - 1\right].
\end{aligned} \tag{14}$$

Expanding Equation 14 by plugging in Equation 10 results in

$$\begin{aligned}
\mathcal{F}_1(t) &= 1 + K_{11}\tanh\left(\frac{\gamma_1\int_{t-\tau_1-1}^{t-\tau_1}(1-\mathcal{F}_1(s))ds}{K_{11}\mathcal{F}_1(t-\tau_1-1)}\right) + \phi_{12}\left[K_{12}\tanh\left(\frac{\gamma_2\int_{t-\tau_2-1}^{t-\tau_2}(1-\mathcal{F}_2(s))ds}{K_{12}\mathcal{F}_2(t-\tau_2-1)}\right)\right] \\
\mathcal{F}_2(t) &= 1 + K_{12}\tanh\left(\frac{\gamma_2\int_{t-\tau_2-1}^{t-\tau_2}(1-\mathcal{F}_2(s))ds}{K_{12}\mathcal{F}_2(t-\tau_2-1)}\right) + \phi_{12}\left[K_{11}\tanh\left(\frac{\gamma_1\int_{t-\tau_1-1}^{t-\tau_1}(1-\mathcal{F}_1(s))ds}{K_{11}\mathcal{F}_1(t-\tau_1-1)}\right)\right] \\
&\quad + \phi_{23}\left[K_{13}\tanh\left(\frac{\gamma_3\int_{t-\tau_3-1}^{t-\tau_3}(1-\mathcal{F}_3(s))ds}{K_{13}\mathcal{F}_3(t-\tau_3-1)}\right)\right] \\
\mathcal{F}_3(t) &= 1 + K_{13}\tanh\left(\frac{\gamma_3\int_{t-\tau_3-1}^{t-\tau_3}(1-\mathcal{F}_3(s))ds}{K_{13}\mathcal{F}_3(t-\tau_3-1)}\right) \\
&\quad + \phi_{23}\left[K_{12}\tanh\left(\frac{\gamma_2\int_{t-\tau_2-1}^{t-\tau_2}(1-\mathcal{F}_2(s))ds}{K_{12}\mathcal{F}_2(t-\tau_2-1)}\right)\right].
\end{aligned} \tag{15}$$

Each nephron is associated with its own time delay τ_1, τ_2, and τ_3; its own gain γ_1, γ_2, and γ_3; as well as its own range of feedback response, K_{11}, K_{12}, and K_{13}.

If the three coupled nephrons system is perturbed (simulated by adding a small quantity to the right hand side of one of the flows in Equation 15), the flow either returns to a stable steady state or is replaced by stable limit-cycle oscillations. We proceed to analyze the system focusing on the effects of asymmetric coupling using both analytical and numerical methods.

4 Bifurcation Analysis

Bifurcation analysis begins by linearizing Equation 15 about the steady state solution $\mathcal{F}_i = 1$ for $i = 1, 2, 3$, assuming that each $\mathcal{F}_i$ is a small deviation from the steady state flow as in the form

$$\mathcal{F}_i(t) = 1 + \epsilon D_i(t), \qquad \text{for } i = 1, 2, 3. \tag{16}$$

Substituting Equation 16 into Equation 15 and simplifying, the following is obtained,

$$\begin{aligned}
\epsilon D_1(t) &= K_{11} \tanh\left(\frac{-\gamma_1 \int_{t-\tau_1-1}^{t-\tau_1} \epsilon D_1(s)ds}{K_{11}(1+\epsilon D_1(t-\tau_1-1))}\right) + \phi_{12}\left[K_{12}\tanh\left(\frac{-\gamma_2 \int_{t-\tau_2-1}^{t-\tau_2} \epsilon D_2(s)ds}{K_{12}(1+\epsilon D_2(t-\tau_2-1))}\right)\right] \\
\epsilon D_2(t) &= K_{12} \tanh\left(\frac{-\gamma_2 \int_{t-\tau_2-1}^{t-\tau_2} \epsilon D_2(s)ds}{K_{12}(1+\epsilon D_2(t-\tau_2-1))}\right) + \phi_{12}\left[K_{11}\tanh\left(\frac{-\gamma_1 \int_{t-\tau_1-1}^{t-\tau_1} \epsilon D_1(s)ds}{K_{11}(1+\epsilon D_1(t-\tau_1-1))}\right)\right] \\
&\quad +\phi_{23}\left[K_{13}\tanh\left(\frac{-\gamma_3 \int_{t-\tau_3-1}^{t-\tau_3} \epsilon D_3(s)ds}{K_{13}(1+\epsilon D_3(t-\tau_3-1))}\right)\right] \\
\epsilon D_3(t) &= K_{13} \tanh\left(\frac{-\gamma_3 \int_{t-\tau_3-1}^{t-\tau_3} \epsilon D_3(s)ds}{K_{13}(1+\epsilon D_3(t-\tau_3-1))}\right) \\
&\quad +\phi_{23}\left[K_{12}\tanh\left(\frac{-\gamma_2 \int_{t-\tau_2-1}^{t-\tau_2} \epsilon D_2(s)ds}{K_{12}(1+\epsilon D_2(t-\tau_2-1))}\right)\right].
\end{aligned} \tag{17}$$

Then using the binomial expansion approximation $\frac{1}{1+\epsilon D_i(x)} \approx 1 - \epsilon D_i(x)$, the Taylor Series approximation $\tanh(x) \approx x$, expanding the system in ϵ, and retaining first order terms results in

$$\begin{aligned}
D_1(t) &= -\gamma_1 \int_{t-\tau_1-1}^{t-\tau_1} D_1(s)ds - \phi_{12}\gamma_2 \int_{t-\tau_2-1}^{t-\tau_2} D_2(s)ds \\
D_2(t) &= -\gamma_2 \int_{t-\tau_2-1}^{t-\tau_2} D_2(s)ds - \phi_{12}\gamma_1 \int_{t-\tau_1-1}^{t-\tau_1} D_1(s)ds - \phi_{23}\gamma_3 \int_{t-\tau_3-1}^{t-\tau_3} D_3(s)ds \\
D_3(t) &= -\gamma_3 \int_{t-\tau_3-1}^{t-\tau_3} D_3(s)ds - \phi_{23}\gamma_2 \int_{t-\tau_2-1}^{t-\tau_2} D_2(s)ds.
\end{aligned} \tag{18}$$

We now look for solutions of the form

$$D_i(t) = d_i e^{\lambda t}, \qquad \text{for } i = 1, 2, 3, \tag{19}$$

where d_1, d_2, and d_3 are constants. Because λ can have a real and imaginary part, $e^{\lambda t}$ can modify the amplitude of D_i and allow oscillations in D_i. If $Re(\lambda) < 0$, then $D \to 0$ and a perturbation ultimately decays, returning the system to a steady state. If $Re(\lambda) > 0$, then a perturbation grows – in principle, without bound. In practice, nonlinearities in the system modulate the runaway growth. If in addition, $Im(\lambda) \neq 0$, finite amplitude oscillations result, a so-called Hopf bifurcation. After substituting Equation 19 into Equation 18, integrating, and canceling the factor $e^{\lambda t}$, the

following linear system of equations is obtained,

$$\begin{pmatrix} \lambda+\gamma_1(e^{-\lambda\tau_1}-e^{-\lambda(\tau_1+1)}) & \phi_{12}\gamma_2(e^{-\lambda\tau_2}-e^{-\lambda(\tau_2+1)}) & 0 \\ \phi_{12}\gamma_1(e^{-\lambda\tau_1}-e^{-\lambda(\tau_1+1)}) & \lambda+\gamma_2(e^{-\lambda\tau_2}-e^{-\lambda(\tau_2+1)}) & \phi_{23}\gamma_3(e^{-\lambda\tau_3}-e^{-\lambda(\tau_3+1)}) \\ 0 & \phi_{23}\gamma_2(e^{-\lambda\tau_2}-e^{-\lambda(\tau_2+1)}) & \lambda+\gamma_3(e^{-\lambda\tau_3}-e^{-\lambda(\tau_3+1)}) \end{pmatrix} \begin{pmatrix} d_1 \\ d_2 \\ d_3 \end{pmatrix} = \begin{pmatrix} 0 \\ 0 \\ 0 \end{pmatrix}. \tag{20}$$

This system of linear equations will have nontrivial solutions only if the determinant of the coefficient matrix is zero. The characteristic equation can be found by solving the determinant, set equal to zero, for λ in terms of the other parameters. Solving this determinant explicitly is challenging, so a method for reducing the number of parameters is introduced to better understand the behavior of the system.

4.1 Reduction of Parameters

To make solving the determinant of the coefficient matrix in Equation 20 more manageable, the following assumptions were made regarding the behavior of the time delays, gains, and coupling constants among the nephrons. First, the time delays, τ, are set as equal for each nephron (an idealized situation). The gains are averaged such that the three are written as a constant, γ_0, and that constant plus or minus a small change, $\gamma_0 \pm \delta$, since the gains are physiologically similar enough among nephrons. The coupling constants are also averaged such that they are written as a constant plus or minus a small change, $\phi_0 \pm \eta$. Therefore, the three nephrons are very similar, but their difference is characterized through slightly varying parameter values.

In this study, it was assumed that the largest gain and the largest coupling would occur upstream in the cortical radial artery (nephron 1) and the smallest gain and the smallest coupling would occur downstream in the cortical radial artery (nephron 3) while the average value of gain would occur in the middle (nephron 2) (see Figure 3). Hence,

$$\begin{aligned} \gamma_1 &= \gamma_0+\delta \\ \gamma_2 &= \gamma_0 \\ \gamma_3 &= \gamma_0-\delta \\ \phi_{12} &= \phi_0+\eta \\ \phi_{23} &= \phi_0-\eta \\ \tau &= \tau_1=\tau_2=\tau_3. \end{aligned}$$

Plugging the newly defined parameters into Equation 15, the coefficient matrix of the system, after setting $E = e^{-\lambda\tau} - e^{-\lambda(\tau+1)}$ to simplify for visual purposes, becomes

$$\begin{pmatrix} \lambda+(\gamma_0+\delta)E & (\phi_0+\eta)\gamma_0 E & 0 \\ (\phi_0+\eta)(\gamma_0+\delta)E & \lambda+\gamma_0 E & (\phi_0-\eta)(\gamma_0-\delta)E \\ 0 & (\phi_0-\eta)\gamma_0 E & \lambda+(\gamma_0-\delta)E \end{pmatrix}. \tag{21}$$

The determinant equation is

$$\begin{aligned} \big(\lambda+(\gamma_0+\delta)E\big)\Big[\big(\lambda+\gamma_0 E\big)\big(\lambda+(\gamma_0-\delta)E\big)-\big((\phi_0-\eta)(\gamma_0-\delta)E\big)\big((\phi_0-\eta)\gamma_0 E\big)\Big] \\ -\big((\phi_0+\eta)\gamma_0 E\big)\Big[\big((\phi_0+\eta)(\gamma_0+\delta)E\big)\big(\lambda+(\gamma_0-\delta)E\big)\Big]=0, \end{aligned} \tag{22}$$

which is still a bit unwieldy to solve analytically, so the subsequent sections simplify the determinant

to a very basic form, and then slowly add in complexity in hopes of arriving at the solution to Equation 22.

4.1.1 Identical Nephrons

In the case where the gains in each of the three nephrons are the same ($\delta = 0$), and there is no coupling constant ($\phi_0 = \eta = 0$), the determinant, after simplifying, becomes

$$E^3{\gamma_0}^3 + 3\lambda E^2{\gamma_0}^2 + 3\lambda^2 E\gamma_0 + \lambda^3 = 0. \tag{23}$$

This equation can be solved for γ_0; the roots of the solution are:

$$\gamma_0 = -\frac{\lambda}{E}, \quad -\frac{\lambda}{E}, \quad -\frac{\lambda}{E}. \tag{24}$$

In this case, the three roots are identical because the nephrons are identical, independent, and not coupled, so three copies of the characteristic equation for a single nephron should be the result.

Using one of the roots, we can easily see that

$$-\gamma_0\frac{E}{\lambda} = 1, \tag{25}$$

and remembering the substitution $E = e^{-\lambda\tau} - e^{-\lambda(\tau+1)}$, which also equals $-e^{-\lambda\tau}(e^{-\lambda} - 1)$, we result in the characteristic equation,

$$\gamma_0 e^{-\lambda\tau}\left(\frac{e^{-\lambda} - 1}{\lambda}\right) = 1, \tag{26}$$

which was originally determined by Layton *et al.* (1991).

Letting $\lambda = i\omega$, Equation 26 becomes

$$-i\gamma_0 e^{-i\omega\tau}(e^{-i\omega} - 1) = \omega. \tag{27}$$

Using the definition $e^{i\omega} = \cos(\omega) + i\sin(\omega)$, expanding the equation, and then using the trigonometric identities $\cos(x+y) = \cos(x)\cos(y) - \sin(x)\sin(y)$ and $\sin(x+y) = \cos(x)\sin(y) + \cos(y)\sin(x)$, Equation 27 becomes

$$-i\gamma_0\big[\cos(\omega\tau + \omega) - i\sin(\omega\tau + \omega) - \cos(\omega\tau) + i\sin(\omega\tau)\big] = \omega. \tag{28}$$

Substituting $\omega\tau + \omega = \omega\left(\tau + \frac{1}{2}\right) + \frac{\omega}{2}$ and $\omega\tau = \omega\left(\tau + \frac{1}{2}\right) - \frac{\omega}{2}$, expanding using the trigonometric identities identified previously, and then after utilizing some algebra, the result is

$$-\gamma_0\sin\left(\frac{\omega}{2}\right)\left[\cos\left(\omega\left(\tau + \frac{1}{2}\right)\right) - i\sin\left(\omega\left(\tau + \frac{1}{2}\right)\right)\right] = \frac{\omega}{2}. \tag{29}$$

The imaginary part of Equation 29,

$$\gamma_0\sin\left(\frac{\omega}{2}\right)\sin\left(\omega\left(\tau + \frac{1}{2}\right)\right) = 0, \tag{30}$$

implies that either $\frac{\omega}{2} = n\pi$ or $\omega(\tau + \frac{1}{2}) = n\pi$, $n = 1, 2, 3, \ldots$. Substituted into Equation 29, $\frac{\omega}{2} = n\pi$ implies that $\omega = 0$ and $n = 0$, corresponding to the steady state solution. Plugging $\omega(\tau + \frac{1}{2}) = n\pi$

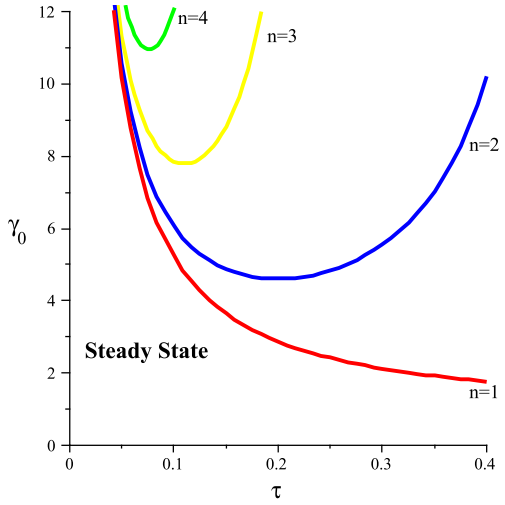

Figure 4: Bifurcation curves – identical nephrons: Given by Equation 32, γ_{0_n} for $n = 1, 2, 3, 4$. In the "Steady State" region, a solution obtained by a perturbation of the steady state solution will converge back to the steady state solution. Above the "n=1" curve (primary bifurcation curve), a solution obtained by a perturbation of the steady state solution will result in stable limit-cycle oscillations.

into the real part of Equation 29 results in

$$\gamma_0 \sin\left(\frac{n\pi}{2\tau+1}\right)\cos(n\pi) = \frac{n\pi}{2\tau+1}, \qquad n = 1, 2, 3, \ldots, \tag{31}$$

which, after some algebra and the equality $\cos(n\pi) = (-1)^{n+1}$, $n = 1, 2, 3, \ldots$, ultimately results in an equation that defines bifurcation curves in the positive γ_0–τ plane corresponding to time-dependent oscillatory solutions,

$$\gamma_{0_n} = (-1)^{n+1}\frac{n\pi/(2\tau+1)}{\sin(n\pi/(2\tau+1))}, \qquad n = 1, 2, 3, \ldots. \tag{32}$$

The bifurcation curve when $n = 1$ is γ_{0_1}, which is referred to as the "primary bifurcation curve." Below this curve, as visualized in Figure 4, the flows of the three nephrons return to a steady state, and above the bifurcation curve the flows are replaced by an oscillating state. Referring to Equation 19, this follows from $Re(\lambda) < 0$ implies decaying oscillations and $Re(\lambda) > 0$ implies growing oscillations. Therefore, crossing the primary bifurcation curve results in a Hopf bifurcation. Crossing the bifurcation curve when $n = 2$ (γ_{0_2}) results in higher order oscillations, perhaps including beats. Curves defined when $n = 3$ (γ_{0_3}), $n = 4$ (γ_{0_4}), and so on indicate more complex oscillations. The primary bifurcation curve is the focus of this bifurcation analysis.

4.1.2 Differing Gains, No Coupling

In the case where there is no coupling constant ($\phi_0 = \eta = 0$), the determinant, after simplifying, becomes

$$E^3{\gamma_0}^3 + 3\lambda E^2{\gamma_0}^2 + (3\lambda^2 E - \delta^2 E^3)\gamma_0 + \lambda^3 - \lambda\delta^2 E^2 = 0. \tag{33}$$

This equation can be solved for γ_0; the roots of the solution are:

$$\gamma_0 = -\frac{\lambda}{E}, \quad \frac{-\lambda + \delta E}{E}, \quad \frac{-\lambda - \delta E}{E}. \tag{34}$$

The first root is the same as found in Section 4.1.1. The second root may be written as

$$\frac{\gamma_0 E}{-\lambda + \delta E} = 1, \tag{35}$$

which after algebraic simplification becomes

$$-(\gamma_0 - \delta)\frac{E}{\lambda} = 1, \tag{36}$$

and following the substitution made in Equation 26, where for a parameter C (we begin to notice a pattern here),

$$-C\frac{E}{\lambda} = 1 \quad \Longrightarrow \quad Ce^{-\lambda\tau}\left(\frac{e^{-\lambda}-1}{\lambda}\right) = 1, \tag{37}$$

the characteristic equation is

$$(\gamma_0 - \delta)e^{-\lambda\tau}\left(\frac{e^{-\lambda}-1}{\lambda}\right) = 1. \tag{38}$$

Following the same steps as in the previous section (Equations 26-32), where for a parameter C,

$$Ce^{-\lambda\tau}\left(\frac{e^{-\lambda}-1}{\lambda}\right) = 1 \quad \Longrightarrow \quad C_n = (-1)^{n+1}\frac{n\pi/(2\tau+1)}{\sin(n\pi/(2\tau+1))}, \qquad n = 1, 2, 3, \ldots, \tag{39}$$

ultimately results in the equation that defines bifurcation curves in the γ_0–τ–δ space corresponding to time-dependent oscillatory solutions,

$$\gamma_{0n} = (-1)^{n+1}\frac{n\pi/(2\tau+1)}{\sin(n\pi/(2\tau+1))} + \delta, \qquad n = 1, 2, 3, \ldots. \tag{40}$$

The primary bifurcation surface is shown in blue in Figure 5. Note that the flows of the three nephrons return to a steady state for parameter values below the lowest bifurcation surface, which is the red surface given by the third root, and oscillations occur for all parameter values above the lower red surface.

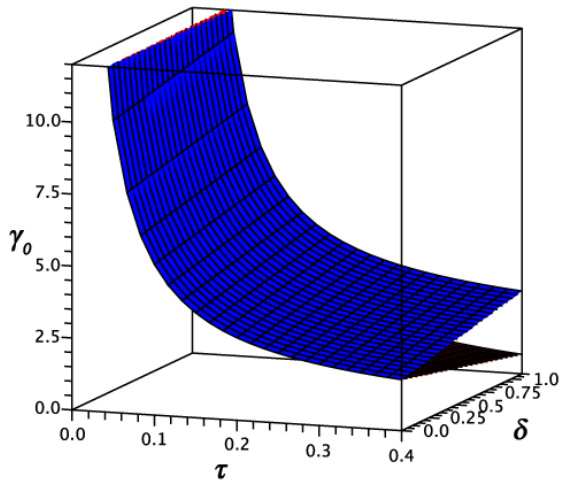

Figure 5: Bifurcation surfaces – differing gains and no coupling: The upper blue primary bifurcation surface is given by root $\gamma_0 = \frac{-\lambda+\delta E}{E}$ and the lower red primary bifurcation surface is given by root $\gamma_0 = \frac{-\lambda-\delta E}{E}$. The "Steady State" region is located near the origin, similar to the bifurcation curves in Figure 4. Above the lower primary bifurcation surface exists the region with stable limit-cycle oscillations.

The third root may be written as

$$\frac{\gamma_0 E}{-\lambda - \delta E} = 1, \tag{41}$$

which after algebraic simplification becomes

$$-(\gamma_0 + \delta)\frac{E}{\lambda} = 1, \tag{42}$$

and following Equation 37, the characteristic equation is

$$(\gamma_0 + \delta)e^{-\lambda\tau}\left(\frac{e^{-\lambda} - 1}{\lambda}\right) = 1. \tag{43}$$

Following the steps in Equation 39, the equation that defines bifurcation curves in the γ_0–τ–δ space corresponding to time-dependent oscillatory solutions is

$$\gamma_{0n} = (-1)^{n+1}\frac{n\pi/(2\tau+1)}{\sin(n\pi/(2\tau+1))} - \delta, \qquad n = 1, 2, 3, \ldots. \tag{44}$$

The primary bifurcation surface is shown in red in Figure 5. Again, because the red bifurcation surface given by the third root is lower than the blue surface given by the second root, below the red surface exists the "Steady State" region and above the red surface exists the region with stable limit-cycle oscillations. In the case of differing gains and no coupling, there is no additional fluid flow into the system because the coupling constant is equal to zero (see Equation 15). There is only a redistribution of fluid, but it can be seen that there is an increased likelihood of oscillations compared to the identical nephron case.

4.1.3 Other Cases

Due to the ease of determining the characteristic equation and the equation that defines bifurcation curves once the roots of the determinant have been found (Equations 37 and 39), we briefly summarize the results for other possible cases.

Identical Gains, Identical Coupling In the case where the gains are identical ($\delta = 0$) and the coupling constants are identical ($\eta = 0$), the determinant, after simplifying, becomes

$$(E^3 - 2{\phi_0}^2E^3){\gamma_0}^3 + (3\lambda E^2 - 2\lambda{\phi_0}^2E^2){\gamma_0}^2 + 3\lambda^2E\gamma_0 + \lambda^3 = 0, \tag{45}$$

and the resulting equations are as follows:

Root	Characteristic Equation
$\gamma_0 = -\frac{\lambda}{E}$	$\gamma_0 e^{-\lambda\tau}\left(\frac{e^{-\lambda}-1}{\lambda}\right) = 1$
$\gamma_0 = -\left(\frac{-1-\sqrt{2}\phi_0}{-1+2{\phi_0}^2}\right)\frac{\lambda}{E}$	$\gamma_0\left(\frac{-1+2{\phi_0}^2}{-1-\sqrt{2}\phi_0}\right)e^{-\lambda\tau}\left(\frac{e^{-\lambda}-1}{\lambda}\right) = 1$
$\gamma_0 = -\left(\frac{-1+\sqrt{2}\phi_0}{-1+2{\phi_0}^2}\right)\frac{\lambda}{E}$	$\gamma_0\left(\frac{-1+2{\phi_0}^2}{-1+\sqrt{2}\phi_0}\right)e^{-\lambda\tau}\left(\frac{e^{-\lambda}-1}{\lambda}\right) = 1$

The primary bifurcation surfaces for both roots are shown in Figure 6. The flows of the three nephrons return to a steady state below the lowest surface and oscillations occur above the lowest surface. It can be seen in the case of identical gains and identical coupling that coupling enhances oscillations compared to the identical nephron case.

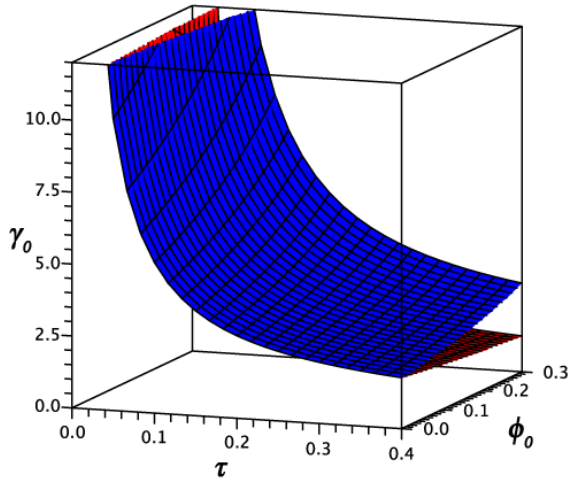

Figure 6: Bifurcation surfaces – identical gains and identical coupling: The upper blue primary bifurcation surface is given by root $\gamma_0 = -\left(\frac{-1-\sqrt{2}\phi_0}{-1+2{\phi_0}^2}\right)\frac{\lambda}{E}$ and the lower red primary bifurcation surface is given by root $\gamma_0 = -\left(\frac{-1+\sqrt{2}\phi_0}{-1+2{\phi_0}^2}\right)\frac{\lambda}{E}$. The "Steady State" region is located near the origin, similar to the bifurcation curves in Figure 4. Above the lower primary bifurcation surface exists the region with stable limit-cycle oscillations.

In the case where the gains are identical ($\delta = 0$) and $\phi_0 = 0$ but $\eta \neq 0$, the same characteristic equations determined in this section would result, substituting η for every instance of ϕ_0. Since the coupling would average as 0, there would be no additional fluid flow into the system, but the fluid would be redistributed. Again, it can be seen in this redistribution model that there is an increased likelihood of oscillations compared to the identical nephron case.

Identical Gains, Differing Coupling In the case where the gains are identical ($\delta = 0$) and the coupling constants are differing, the determinant, after simplifying, becomes

$$(E^3 - 2{\phi_0}^2E^3 - 2\eta^2E^3){\gamma_0}^3 + (3\lambda E^2 - 2\lambda{\phi_0}^2E^2 - 2\lambda\eta^2E^2){\gamma_0}^2 + 3\lambda^2E\gamma_0 + \lambda^3 = 0. \quad (46)$$

and the resulting equations are as follows:

Root	Characteristic Equation
$\gamma_0 = -\frac{\lambda}{E}$	$\gamma_0 e^{-\lambda\tau}\left(\frac{e^{-\lambda}-1}{\lambda}\right) = 1$
$\gamma_0 = -\left(\frac{-1-\sqrt{2({\phi_0}^2+\eta^2)}}{-1+2({\phi_0}^2+\eta^2)}\right)\frac{\lambda}{E}$	$\gamma_0\left(\frac{-1+2({\phi_0}^2+\eta^2)}{-1-\sqrt{2({\phi_0}^2+\eta^2)}}\right)e^{-\lambda\tau}\left(\frac{e^{-\lambda}-1}{\lambda}\right) = 1$
$\gamma_0 = -\left(\frac{-1+\sqrt{2({\phi_0}^2+\eta^2)}}{-1+2({\phi_0}^2+\eta^2)}\right)\frac{\lambda}{E}$	$\gamma_0\left(\frac{-1+2({\phi_0}^2+\eta^2)}{-1+\sqrt{2({\phi_0}^2+\eta^2)}}\right)e^{-\lambda\tau}\left(\frac{e^{-\lambda}-1}{\lambda}\right) = 1$

The bifurcation surfaces are now in four dimensions – impossible to graph without taking cross sections. We look at the endpoints and midpoint of the range of η, where $\eta = 0, 0.0725, 0.1450$. When $\eta = 0$, the result is the same as the result in the previous section, as illustrated in Figure 6. Figure 7a shows the primary bifurcation surfaces for both roots when $\eta = 0.0725$ and Figure 7b illustrates the case when $\eta = 0.1450$. It can be seen in the case of identical gains and differing coupling that asymmetric coupling enhances oscillations compared to the identical nephron case.

Differing Gains, Identical Coupling In the case where the gains are differing and the coupling constants are identical ($\eta = 0$), the determinant, after simplifying, becomes

$$(E^3 - 2{\phi_0}^2E^3){\gamma_0}^3 + (3\lambda E^2 - 2\lambda{\phi_0}^2E^2){\gamma_0}^2 + (3\lambda^2E + 2{\phi_0}^2\delta^2E^3 - \delta^2E^3)\gamma_0 \quad (47)$$
$$-\lambda\delta^2E^2 + \lambda^3 = 0.$$

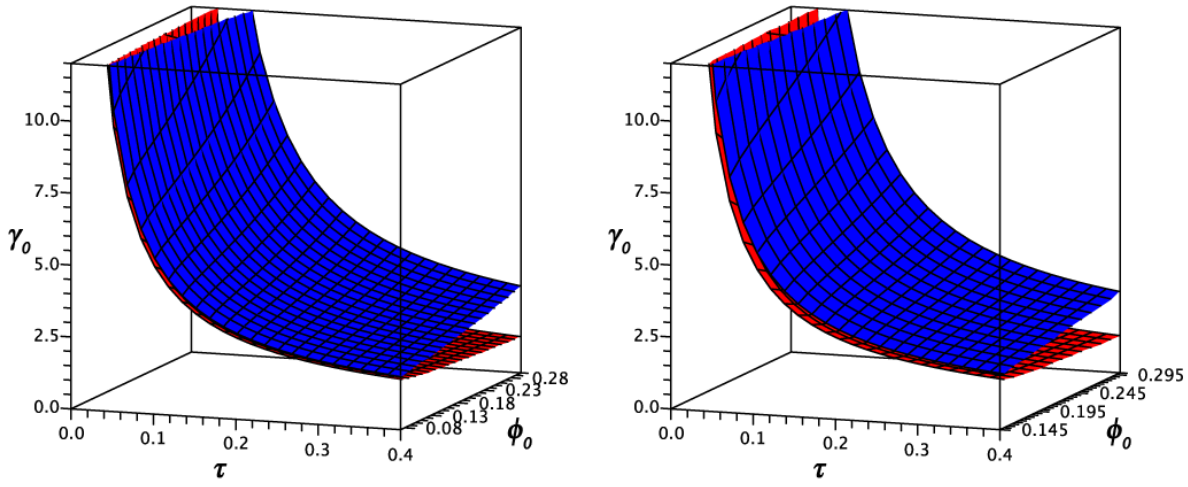

(a) $\eta = 0.0725$ **(b)** $\eta = 0.1450$

Figure 7: Bifurcation surfaces – identical gains and differing coupling: The upper blue primary bifurcation surface is given by root $\gamma_0 = -\left(\frac{-1-\sqrt{2(\phi_0{}^2+\eta^2)}}{-1+2(\phi_0{}^2+\eta^2)}\right)\frac{\lambda}{E}$ and the lower red primary bifurcation surface is given by root $\gamma_0 = -\left(\frac{-1+\sqrt{2(\phi_0{}^2+\eta^2)}}{-1+2(\phi_0{}^2+\eta^2)}\right)\frac{\lambda}{E}$. The "Steady State" region is located near the origin, similar to the bifurcation curves in Figure 4. Above the lower primary bifurcation surface exists the region with stable limit-cycle oscillations.

This equation can be solved for γ_0; however, the roots cannot be expressed in a simplified form. In the case where the gains are differing and $\phi_0 = 0$ but $\eta \neq 0$, the determinant is the same as Equation 47, substituting η for every instance of ϕ_0. It is here that we cease the analytic approach for solving the determinant. We are one step from solving the original equation, Equation 22 with differing gains and differing coupling, yet as we turn to numerical methods we can obtain a very close approximation to the bifurcation surface of the three coupled nephrons system.

5 Numerical Analysis

We begin by analyzing differing flow behaviors after a perturbation in the three coupled nephrons system for varying η and δ, and then sample points throughout the physiologically relevant τ–ϕ_0–γ_0 space to obtain an estimate of the bifurcation surface for the system. The steady state was disturbed by introducing a perturbation of magnitude 1.00001 to the first nephron for 1.5 time units (see Appendix B for an explanation of the MATLAB-implemented algorithm). Recall that the range of physiologically relevant (nondimensional) values for the time delay is $\tau \in [0.13, 0.37]$, the coupling constant is $\phi_0 \in [0.01, 0.30]$, and the gain is $\gamma_0 \in [1.5, 3.6]$.

5.1 Differing Flow Behaviors

5.1.1 Always in an Oscillatory State

Beginning with the most typical parameters for a nephron, $\tau = 0.22$, $\gamma_0 = 3.17$, and $\phi_0 = 0.1$, we notice similar behavior in flow no matter the choices for η and δ such that $\phi_0 \pm \eta$ and $\gamma_0 \pm \delta$ remain in the range of physiologically relevant values. The case of identical coupling constants ($\eta = 0$) and identical gains ($\delta = 0$) is illustrated in Figure 8a, which shows the TAL flow rate for each nephron over time. The flow of the first nephron is colored in blue, the flow of the second

nephron is colored in green, and the flow of the third nephron is colored in red (see Figure 3 for a schematic drawing of the location of each nephron). The flows are symmetric in this case; both the first and third nephrons have the same amplitude (not easily seen in Figure 8a, yet verified by output calculations). The oscillations for each of the nephrons are in sync and their periods are of the same length.

A case with differing coupling constants and gains is illustrated in Figure 8b with $\eta = 0.08$ and $\delta = 0.35$. Here all three nephrons are oscillating in sync again. The flows of the first and third nephrons are not symmetric in this case because the coupling between nephron 1 and 2 ($\phi_0 + \eta = 0.18$) is stronger than the coupling between 2 and 3 ($\phi_0 - \eta = 0.02$), resulting in differing amplitudes. For any η and δ, the three nephrons exhibit oscillatory behavior for the typical case of $\tau = 0.22$, $\gamma_0 = 3.17$, and $\phi_0 = 0.1$.

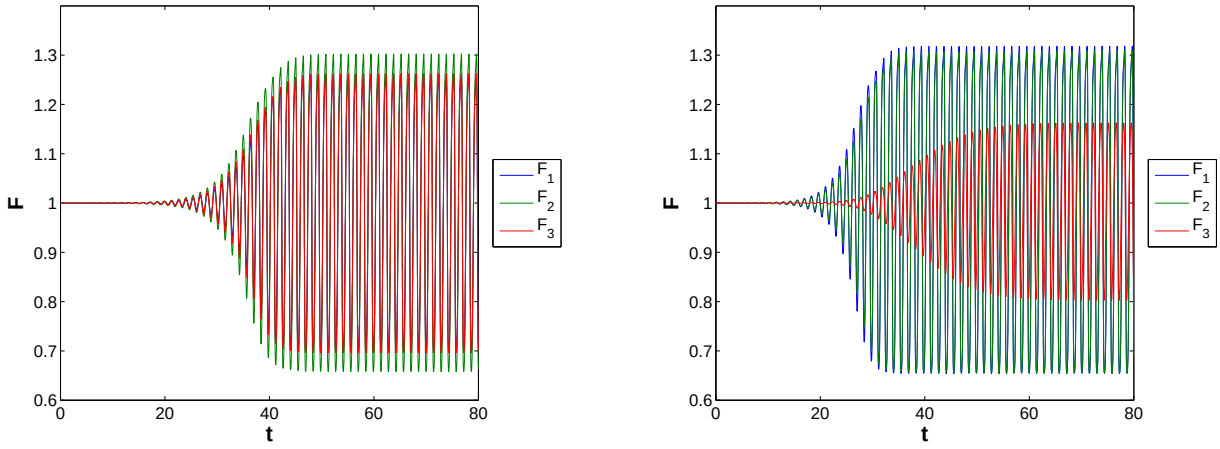

(a) $\eta = 0$, $\delta = 0$ **(b)** $\eta = 0.08$, $\delta = 0.35$

Figure 8: TAL flow rate over time for 3 nephrons: (τ, γ_0, ϕ_0) = (0.22, 3.17, 0.1).

5.1.2 Always in a Steady State

By lowering the value of τ to 0.20 and γ_0 to 2.025, we notice different behavior while keeping $\phi_0 = 0.1$. The case of identical coupling constants ($\eta = 0$) and identical gains ($\delta = 0$) is illustrated in Figure 9a. The flows of each of the three nephrons quickly decay after experiencing an increase in flow due to the perturbation in the first nephron. The amplitude of the first nephron is the largest, followed by the amplitude of the second nephron and then the third.

A case with differing coupling constants and gains is illustrated in Figure 9b with $\eta = 0.08$ and $\delta = 0.50$. The nephron flows decay again after the perturbation, but more slowly this time. The relative differences in amplitude between the three nephrons are the same as compared to the case with identical coupling constants and gains. The actual amplitude of the first and third nephrons appear to be the same in both cases. The actual amplitude of the second nephron is larger in the differing coupling constants and gains case. In general, for any set of η and δ, the three nephrons result in steady state behavior for the case of $\tau = 0.20$, $\gamma_0 = 2.025$, and $\phi_0 = 0.1$.

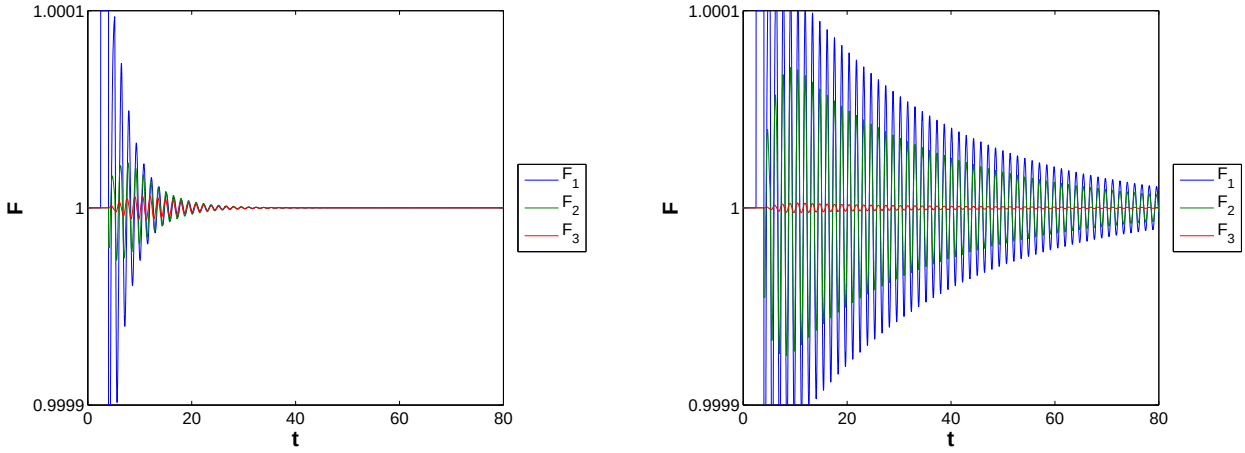

(a) $\eta = 0$, $\delta = 0$ **(b)** $\eta = 0.08$, $\delta = 0.50$

Figure 9: TAL flow rate over time for 3 nephrons: $(\tau, \gamma_0, \phi_0) = (0.20, 2.025, 0.1)$.

5.1.3 Either in a Steady State or an Oscillatory State

After lowering the value of τ to 0.18, increasing the value of γ_0 to 2.55, and keeping $\phi_0 = 0.1$, another set of behavior occurs. The case of identical coupling constants ($\eta = 0$) and identical gains ($\delta = 0$) is illustrated in Figure 10a. Similar to Section 5.1.2, the flows of each nephron quickly decay. The amplitude of the third nephron is the smallest while the first nephron has the largest amplitude and the second nephron's amplitude is in the middle.

A case with differing coupling constants and gains is illustrated in Figure 10b with $\eta = 0.08$ and $\delta = 0.95$. Dissimilar to both of the previous results, the flows of the nephrons do not follow the same pattern as the case of identical coupling constants and gains. Instead, differing the coupling constants and gains results in oscillatory behavior. The flows of the first and third nephron are not

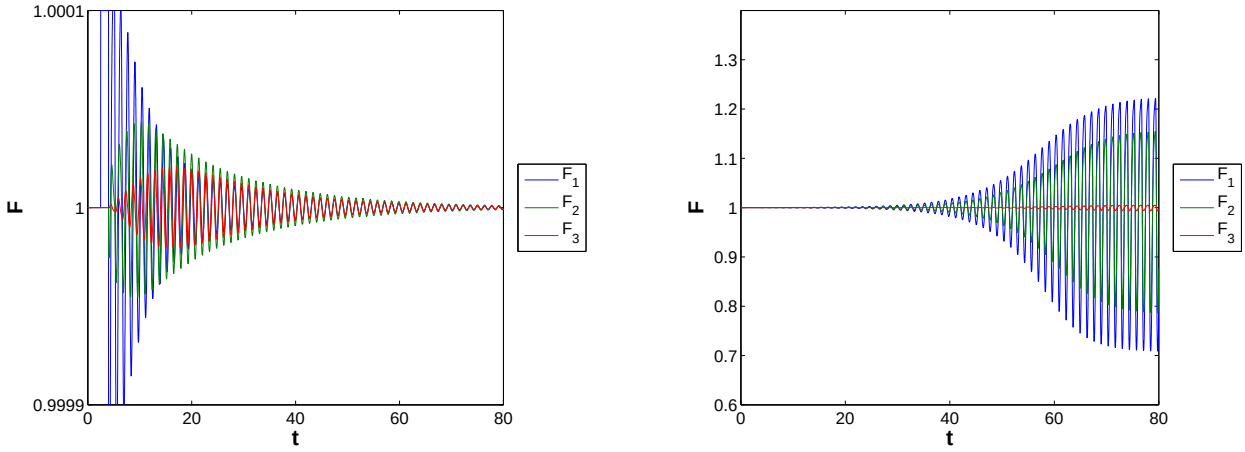

(a) $\eta = 0$, $\delta = 0$ **(b)** $\eta = 0.08$, $\delta = 0.95$

Figure 10: TAL flow rate over time for 3 nephrons: $(\tau, \gamma_0, \phi_0) = (0.18, 2.55, 0.1)$.

symmetric in this case; the third nephron has a very small amplitude but is still oscillating in sync with the other nephrons. The amplitude of the first nephron remains the largest, followed by the second nephron and then the third. In the case of $\tau = 0.18$, $\gamma_0 = 2.55$, and $\phi_0 = 0.1$, there is a Hopf bifurcation in the η–δ plane from steady state behavior to oscillatory behavior.

One can sketch surface plots of the amplitude of TAL flow rate over time depending on η and δ. The final maximum amplitude of nephron 1 is sketched; while the amplitudes of nephron 2 and 3 are not the same as nephron 1 in all cases, the behavior of each nephron at each point in the η–δ plane is the same. One image can represent the three images that would otherwise be produced.

For the case where the flows are always in an oscillatory state, Figure 11a shows that the amplitude is always greater than 1. When the flows are always in a steady state, Figure 11b shows that the amplitude is always equal to 1. When there is a bifurcation in the η–δ plane and flows are either in a steady state or oscillatory state, Figure 11c shows that the amplitude is equal to 1 for small values of η and δ, and there is a distinct location where for larger values of η and δ the amplitude becomes greater than 1. As the value of η increases, the value of δ at which the amplitude becomes larger than 1 decreases. The growth of the amplitude of the oscillating solutions is similar to $\sqrt{\delta}$ for any η.

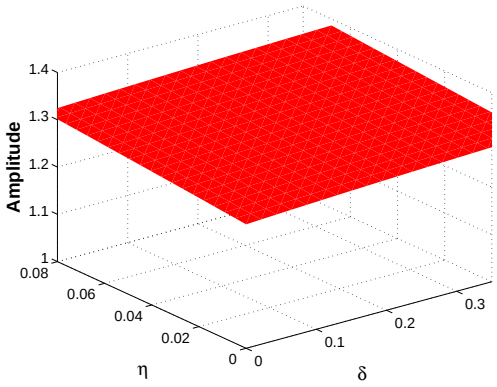

(a) $\tau = .22$, $\gamma = 3.17$, $\phi = 0.1$

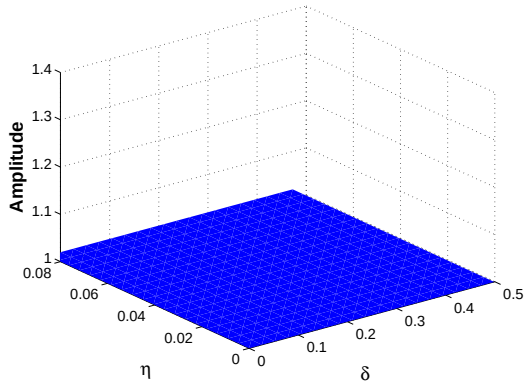

(b) $\tau = .20$, $\gamma = 2.025$, $\phi = 0.1$

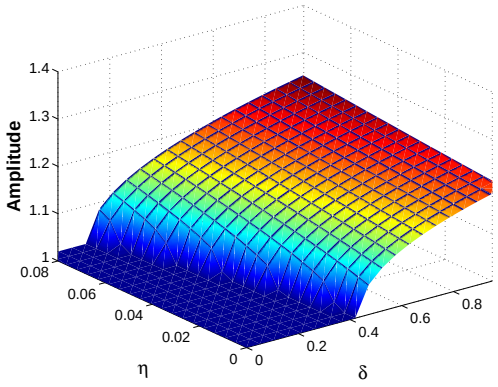

(c) $\tau = .18$, $\gamma = 2.55$, $\phi = 0.1$

Figure 11: TAL flow rates amplitude: (a) Always in an oscillatory state (indicated by red shading); (b) Always in a steady state (indicated by blue shading); (c) Either in a steady state (indicated by blue shading) or an oscillatory state (indicated by a gradient from lighter blue to red shading).

5.2 General Results

The three oscillatory behaviors described above encompass the only behaviors that occur in the τ–ϕ_0–γ_0 plane: all three nephron flows resulting in an oscillatory state for any combination of η and δ, all three nephron flows resulting in a steady state for any combination of η and δ, and all three nephron flows resulting in either a steady state or oscillatory state depending on the combination of η and δ, with a bifurcation through the η–δ plane.

One may ask then, can we numerically determine the flow behavior of three coupled nephrons at any location in the τ–ϕ_0–γ_0 plane?

We divide each of the physiologically relevant intervals for the time delay ($\tau \in [0.13, 0.37]$), coupling constant ($\phi_0 \in [0.01, 0.30]$), and gain ($\gamma_0 \in [1.5, 3.6]$) into smaller equally spaced intervals, and evaluate the behavior at each point. Including the end points in the interval of τ, and dividing into smaller intervals of 0.01 each, 25 values can be evaluated at. For both ϕ_0 and γ_0, the end points of the intervals cannot be used in numerical calculations because the values of $\phi_0 \pm \eta$ and $\gamma_0 \pm \delta$ must also remain in the range of physiologically relevant values. As a result, we divide the intervals of ϕ_0 and γ_0 into 16 smaller intervals and use the 15 end points of each of those intervals as values to evaluate at. Ultimately, a $25 \times 15 \times 15$ grid is created, and the flow behavior at each of the 5625 total points can be evaluated to visually show the numerical results of attempting to locate the bifurcation surface.

The distinct behavior at each point is determined by analyzing the amplitudes and periods of the TAL flow rates over time of the three nephrons for each combination of η and δ. If the amplitude for every (η, δ) combination is equal to 1, the steady state value, for each nephron, then the point is specified to have "steady state behavior." If the amplitude for every (η, δ) combination is greater than 1 for each nephron, the point is specified to have "oscillatory behavior." If the amplitude for some (η, δ) combinations is equal to 1 (always for smaller values of η and δ), and the amplitude for other (η, δ) combinations is greater than 1 (always for larger values of η and δ), the point is specified to have a "bifurcation."

The results of this analysis are displayed in Figure 12. Steady state behavior exists generally for combinations of small values of (τ, ϕ_0, γ_0), oscillatory behavior exists generally for combinations of large values of (τ, ϕ_0, γ_0), and in the middle of the steady state and oscillatory regions exists a region of points that have bifurcations in the η–δ plane. Immediately it can be seen from Figure 12 that at a majority of points, oscillatory behavior is exhibited.

Since bifurcations in a 3-dimensional region are planes and have area, but are not regions themselves and do not have volume, the green bifurcation region in Figure 12 is not the bifurcation

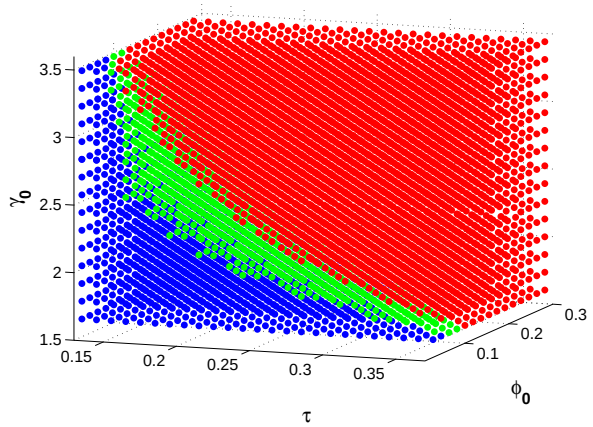

Figure 12: Discrete plot of flow behavior: Blue dots represent steady state behavior, green dots represent bifurcations in the η–δ plane, and red dots represent oscillatory behavior.

of the three coupled nephrons system. Yet, the bifurcation most likely occurs in that region; the discrete numerical approximation results in a low-resolution definition of the bifurcation surface, which is not as exact as might be found analytically. Figure 13 shows the surface plots of the largest values in the steady state region and the smallest values in the oscillatory region; hence, the discrete boundaries of the regions are specified. Finding the average value of these two surfaces, shown in Figure 14, is a close approximation of the primary bifurcation surface of the three coupled nephrons system.

Comparing Figure 14 to the primary bifurcation surfaces in Section 4 (Figures 4, 5, 6, and 7a-b), it can be seen that the bifurcation surface for the three asymmetrically coupled nephrons is either the same or lower than the primary bifurcation surfaces in the other systems. As a result, it can be concluded that three nephrons asymmetrically coupled together are more likely to exhibit limit-cycle oscillations compared to uncoupled nephrons.

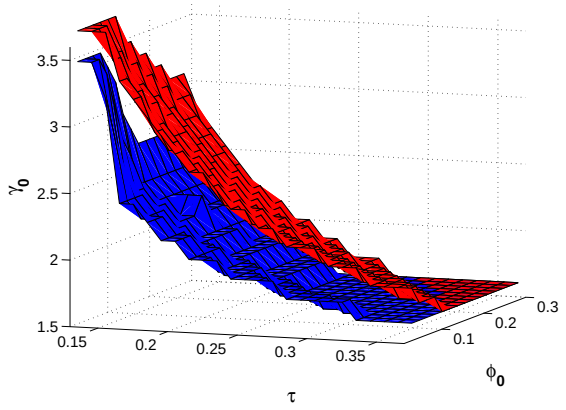

Figure 13: Approximation to the bifurcation curve: Boundaries of the steady state and oscillatory regions: – The blue surface indicates the upper boundary of the steady state region and the red surface indicates the lower boundary of the oscillatory region.

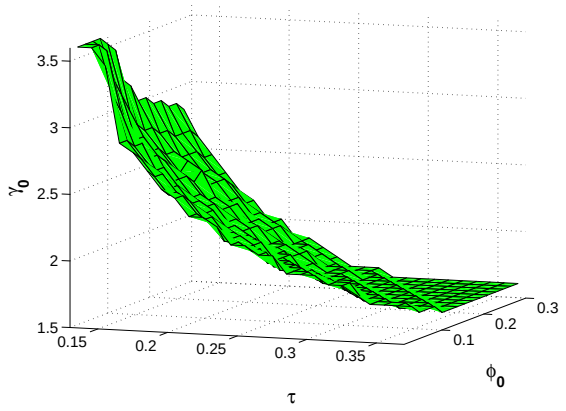

Figure 14: Approximation to the bifurcation curve: Midpoint – This represents a close approximation to the actual primary bifurcation surface of the three coupled nephrons system.

6 Physiological Interpretation

The major functions of the kidneys include the regulation of volume, osmolarity, mineral composition, and acidity of the body, along with the excretion of metabolic waste products and foreign chemicals by processing blood. TGF serves a role in renal autoregulation by primarily regulating glomerular filtration rate with the stabilization of renal blood flow as a consequence because glomerular filtration rate is related to blood pressure and blood flow rate. Large changes in solute

and water excretion are inhibited, and perturbations in arterial blood pressure are prevented from causing major blood flow changes. TGF is most affected not by changes in blood pressure, but by disease or drug-induced blockade of fluid reabsorption in the proximal tubule.

Physiological experiments and measurements in single nephron glomerular filtration rate, TAL fluid chloride concentration, tubular fluid flow rate, and intratubular fluid pressure in normotensive rats show either relatively constant values or regular oscillations with a frequency of 20-50 mHz. Mathematical modeling has helped clarify how these oscillations originate, but physiologists and mathematicians are currently uncertain about the impact of oscillations on renal function, even after more than 20 years of study.

The physiological significance could be that oscillations enhance renal sodium excretion (Layton *et al.*, 2000 and Oldson *et al.*, 2003). This hypothesis is based on predictions that oscillations may enhance sodium delivery to the distal tubule and that oscillations limit the ability of the TGF system to compensate for perturbations in flow, e.g. due to changes in arterial blood pressure. Possible causes of excessive urinary sodium excretion include chronic renal failure, solute diuresis, and aldosterone (a sodium reabsorption hormone) deficiency states such as Addison's disease (Reineck and Stein, 1990). However, more detrimental disorders with many more clinical cases are characterized by excessive sodium retention, such as liver cirrhosis, heart failure, nephrotic syndrome, acute glomerulonephritis, and idiopathic edema. If the aforementioned predictions have an effect on renal function *in vivo*, then the recruitment and entrainment of nephron flow rate oscillations would increase renal sodium excretion.

7 Conclusions

Interactions between nephrons were investigated by determining the effects of asymmetric coupling between three nephrons in an extension of the single nephron integral model. Parameters were chosen so that the gains and coupling constants are averaged while the time delays are equal for each nephron. The largest gain and coupling occurred upstream in the cortical radial artery while the smallest gain and coupling occurred downstream. By varying the parameters of the three coupled nephrons model, it was determined that asymmetric coupling led to an increase in the existence of oscillations, relative to uncoupled nephrons.

It was discovered that the oscillations of the three asymmetrically coupled nephrons under the linearization utilized in this study remained in phase at the same frequency, consistent with previous studies of symmetrically coupled nephrons (Pitman *et al.*, 2004; Bayram 2006). The principal determinant of the frequency of oscillations is the time delay, which is equal for all nephrons in this study. However, gain can contribute to the frequency since it is a measure of change in TAL flow in response to change in macula densa chloride concentration (Layton *et al.*, 1991). Moreover, in-phase synchronization is not an immediate consequence of the delay, since each nephron was perturbed at different times and in different ways. A perturbation in one nephron led to the recruitment and entrainment of the other two nephrons in the system. Therefore, the flow synchronizations in coupled nephrons may be an addition to the growing list of biological synchronous oscillators, such as the flashing of certain species of fireflies in South East Asia, crickets chirping, and cells in the heart beating.

Future studies of the three coupled nephrons model will focus on more complex coupling between nephrons; for example, examining the effects of asymmetric coupling under the assumption that the coupling constant between nephron 1 and nephron 2 is *not* equal to the coupling constant between nephron 2 and nephron 1. Also, redefining the extent of coupling and distribution of flow rates is another aspect that will be investigated.

Acknowledgements

This work was completed and appears in the author's undergraduate honors thesis in partial fulfillment of the requirements for the University at Buffalo Honors Program in Mathematics and the University at Buffalo Honors College. It was supported in part by the National Science Foundation through Grant No. 0616345 to E. Bruce Pitman.

Appendix A

Kidney Excretion and Reabsorption The kidneys regulate blood composition by removing waste. Metabolic waste products that are excreted include urea (from protein), uric acid (from nucleic acid), and creatinine (from muscle creatine). Foreign chemicals that are excreted include drugs, pesticides, and food additives.

Important substances that are reabsorbed back into the general circulation include water, sodium, chloride, calcium, proteins, peptides, phosphate, and sulfate. Hormones that are produced by the kidneys include 1,25-dihydroxyvitamin D_3 (the active form of vitamin D), erythropoietin (involved in red blood cell production), and renin (a component of the renin-angiotensin system which increases arterial blood pressure and causes sodium retention).

Blood Supply Blood enters the kidneys through the renal artery, which branches into gradually smaller arteries – first interlobar arteries, then arcuate arteries, then cortical radial arteries, and then afferent arterioles. Approximately 20% of the blood plasma in the capillaries branching off an afferent arteriole is filtered and the remaining blood returns to general circulation. These capillaries do not form the beginnings of the venous system, but instead recombine to form an efferent arteriole. The efferent arteriole branches into peritubular capillaries, located adjacent to the tubule component of nephrons, which then recombine to form the beginnings of the venous system.

Renal Corpuscle The filtering component of the nephron is called the renal corpuscle. It is comprised of the glomerulus, a tuft of capillaries, which is surrounded by Bowman's capsule. Glomerular filtration is the first part of the process of urine formation. On average, the entire volume of human blood is filtered by the kidneys 60 times per day.

Proximal Tubule After the fluid has been filtered in the renal corpuscle, the filtrate enters the proximal tubule. The proximal tubule is highly permeable to water, and approximately 65% of the water in the fluid is reabsorbed by means of diffusion from the tubule to the peritubular capillary plasma. 65% of the sodium and chloride in the fluid are reabsorbed by active transport in the proximal tubule. The proportion of water, sodium, and chloride reabsorbed in the proximal tubule is approximately equal, yet the volume of water reabsorbed is much greater than the volume of sodium and chloride.

Loop of Henle The Loop of Henle consists of the descending limb and the thick ascending limb (TAL) (and the thin ascending limb in long-looped nephrons). Proportionally, more sodium and chloride is reabsorbed in the entire Loop of Henle than water. In the descending limb, 10% of the water is reabsorbed by diffusion, but there is no active reabsorption of sodium and chloride along

the majority of the length of the descending limb. The osmotic pressure increases four-fold in a long-looped nephron (slightly less in a short-looped nephron) between the beginning and ending of the descending limb – this means that because a lot of water is reabsorbed and solute is not reabsorbed in this portion of the Loop of Henle, the concentration of solute increases. In the TAL, 25% of the sodium and chloride is reabsorbed by means of active transport and diffusion, and water is not reabsorbed. The primary solute in the fluid at the end of the TAL is urea.

Distal Tubule and Collecting Duct Filtrate enters the distal tubule next, where active sodium and chloride reabsorption continues. Approximately 5% of the sodium and chloride is reabsorbed, and the concentration of the filtrate is fine-tuned here. Water does not get reabsorbed in this segment, yet about 5% is reabsorbed (or greater than 24% during dehydration) in the collecting duct, the last major part of the nephron. Water permeability in the collecting duct is controlled by antidiuretic hormone (ADH), and it can be very low or very high. 4-5% of the sodium and chloride is reabsorbed in the collecting duct, and therefore 99-100% of the sodium and chloride that entered the nephron is reabsorbed by the end of the collecting duct while 80-100% of the water is reabsorbed. Urinary concentration occurs as fluid flows from the collecting duct to the renal pelvis.

Appendix B

To determine the behavior of the three coupled nephrons system at each point in the τ–ϕ_0–γ_0 space, two pieces of MATLAB code are run. The first piece of code collects flow rate data and saves it to an array, and the second piece of code loads the array and calculates the amplitudes and periods of the flow rate data.

In the code to collect flow rate data, a loop is used to test points in the η–δ plane for given values of τ, ϕ_0, and γ_0. Below, 20 values of η and 20 values of δ are used and the step size is determined by the algorithm

$$\begin{aligned} \Delta\eta &= \frac{min[abs(\phi_0 - 0.01), abs(0.30 - \phi_0)]}{20} \\ \Delta\delta &= \frac{min[abs(\gamma_0 - 1.5), abs(3.7 - \gamma_0)]}{20}. \end{aligned}$$

A perturbation of magnitude 1.00001 is administered to the first nephron for 1.5 time units. The integrals in Equation 15 are calculated by utilizing the Trapezoid Rule.

The flow rate data from the first piece of code is loaded in the second piece of code to calculate the periods and amplitudes – indicators of steady state or oscillatory state behavior depending on the values. First, indices where the flow rate data crosses the steady state line ($\mathcal{F}(t) = 1$) are placed into an array, and the differences between the indices are calculated. The period is the average of these differences. If the period is equal to 0, then it is assumed that the nephrons are in a steady state. If the period is larger than 0, the flow behavior needs to be determined by analyzing the amplitude. The amplitude is the average of the maximum flow rates within each period. Amplitudes of 1 indicate steady state behavior, and any value larger than 1 (even if by a very small amount) is considered an indicator of oscillatory behavior.

References

M. BARFRED, E. MOSEKILDE and N.-H. HOLSTEIN-RATHLOU (1996). Bifurcation analysis of nephron pressure and flow regulation. *Chaos* **6**, pp. 280–287.

S. BAYRAM (2006). Analysis of TGF-mediated dynamics in a system of many coupled nephrons. Ph.D diss., State University of New York, Buffalo, New York.

D. CASELLAS, M. DUPONT, N. BOURIQUET, L. C. MOORE, A. ARTUSO and A. MIMRAN (1994). Anatomic pairing of afferent arterioles and renin cell distribution in rat kidneys. *Am. J. Physiol.* **267** (*Renal Fluid Electrolyte Physiol.* **36**), pp. F931–F936.

Y.-M. CHEN, K.-P. YIP, D. J. MARSH and N.-H. HOLSTEIN-RATHLOU (1995). Magnitude of TGF-initiated nephron-nephron interaction is increased in SHR. *Am. J. Physiol.* **269** (*Renal Fluid Electrolyte Physiol.* **38**), pp. F198–F204.

N.-H. HOLSTEIN-RATHLOU (1987). Synchronization of proximal intratubular pressure oscillations: evidence for interaction between nephrons. *Pflügers Archiv* **408**, pp. 438-443.

N.-H. HOLSTEIN-RATHLOU and P. P. LEYSSAC (1986). TGF-mediated oscillations in proximal intratubular pressure: Differences between spontaneously hypertensive rats and Wistar-Kyoto rats. *Acta Physiol. Scand.* **126**, pp. 333–339.

N.-H. HOLSTEIN-RATHLOU and P. P. LEYSSAC (1987). Oscillations in the proximal intratubular pressure: a mathematical model. *Am. J. Physiol.* **252** (*Renal Fluid Electrolyte Physiol.* **21**), pp. F560–F572.

N.-H. HOLSTEIN-RATHLOU and D. J. MARSH (1989). Oscillations of tubular pressure, flow, and distal chloride concentration in rats. *Am. J. Physiol.* **256** (*Renal Fluid Electrolyte Physiol.* **25**), pp. F1007–F1014.

N.-H. HOLSTEIN-RATHLOU and D. J. MARSH (1990). A dynamic model of the tubuloglomerular feedback mechanism. *Am. J. Physiol.* **258** (*Renal Fluid Electrolyte Physiol.* **27**), pp. F1448–F1459.

N.-H. HOLSTEIN-RATHLOU and D. J. MARSH (1994). A dynamic model of renal blood flow autoregulation. *Bull. Math. Biol.* **56**, pp. 411–430.

Ö. KÄLLSKOG and D. J. MARSH (1990). TGF-initiated vascular interactions between adjacent nephrons in the rat kidney. *Am. J. Physiol.* **259** (*Renal Fluid Electrolyte Physiol.* **28**), pp. F60–F64.

A. JUST, U. WITTMANN, H. EHMKE and H. R. KIRSCHHEIM (1998). Autoregulation of renal blood flow in the conscious dog and the contribution of the tubuloglomerular feedback. *J. Physiol.* **506.1**, pp. 275–290.

A. T. LAYTON, L. C. MOORE and H. E. LAYTON (2006). Multistability in tubuloglomerular feedback and spectral complexity in spontaneously hypertensive rats. *Am. J. Physiol. Renal Physiol.* **291**, pp. F79-F97.

H. E. LAYTON, E. B. PITMAN and L. C. MOORE (1991). Bifurcation Analysis of TGF-mediated oscillations in SNGFR. *Am. J. Physiol.* **261** (*Renal Fluid Electrolyte Physiol.* **30**), pp. F904–F919.

P. P. LEYSSAC(1986). Further studies on oscillating tubulo-glomerular feedback responses in the rat kidney. *Acta Physiol. Scand.* **126**, pp. 271–277.

P. P. LEYSSAC and L. BAUMBACH (1983). An oscillating intratubular pressure response to alterations in Henle flow in the rat kidney. *Acta Physiol. Scand.* **117**, pp. 415–419.

D. R. OLDSON, L. C. MOORE and H. E. LAYTON (2003). Effect of sustained flow Perturbations on stability and compensation of tubuloglomerular feedback, *Am. J. Physiol. Renal Physiol.* **285**, pp. F972–F989.

E. B. PITMAN, H. E. LAYTON (1989). Tubuloglomerular feedback in a dynamic nephron. *Comm. Pure Appl. Math.* **42**, pp. 759–787.

E. B. PITMAN, R. M. ZARITSKI, L. C. MOORE and H. E. LAYTON (2002). A reduced model for nephron flow dynamics mediated by tubuloglomerular feedback. *Membrane Transport and Renal Physiology*, The IMA Volumes in Mathematics and its Applications **129**, H. E. Layton and A. M. Weinstein (Eds), New York: Springer-Verlag, pp. 345–364.

E. B. PITMAN, R. M. ZARITSKI, K. J. KESSELER, L. C. MOORE, and H. E. LAYTON (2004). Feedback-Mediated Dynamics in Two Coupled Nephrons. *Bull. Math. Bio.* **66**, pp. 1463–1492.

H. J. REINECK, and J. H. STEIN (1990). Disorders of Sodium Metabolism. *Kidney Electrolyte Disorders*, J. C. M. Chan and J. R. Gill (Eds), New York: Churchill Livingstone, pp. 59–105.

J. SCHNERMANN and J. P. BRIGGS (2000). Function of the juxtaglomerular apparatus: control of glomerular hemodynamics and renin secretion. *The Kidney: Physiology and Pathophysiology* (3d ed.), D. W. Seldin and G. Giebisch (Eds), Philadelphia: Lippincott Williams & Wilkins, pp. 945–980.

A. J. VANDER (1995). *Renal physiology.* New York, McGraw-Hill.

K.-P. YIP, N.-H. HOLSTEIN-RATHLOU and D. J. MARSH (1991). Chaos in blood flow control in genetic and renovascular hypertensive rats. *Am. J. Physiol.* **261** (*Renal Fluid Electrolyte Physiol.* **30**), pp. F400–F408.

K.-P. YIP, N.-H. HOLSTEIN-RATHLOU and D. J. MARSH (1992). Dynamics of TGF-initiated nephron-nephron interactions in normotensive rats and SHR. *Am. J. Physiol.* **262** (*Renal Fluid Electrolyte Physiol.* **31**), pp. F980–F988.

R. M. ZARITSKI (1999). Models of Complex Dynamics in Glomerular Filtration Rate. Ph.D diss., State University of New York, Buffalo, New York.